

High-throughput screening and evaluation of double-linker metal-organic frameworks for CO_2/H_2 adsorption and separation

Ji-Long Huang(黄纪龙), Xiu-Ying Liu(刘秀英), Hao Chen(陈浩), Xiao-Dong Li(李晓东), and Jing-Xin Yu(于景新)
Citation: Chin. Phys. B, 2025, 34 (**2**): 027302. DOI: 10.1088/1674-1056/ad925a
Journal homepage: http://cpb.iphy.ac.cn; http://iopscience.iop.org/cpb

What follows is a list of articles you may be interested in

Role of self-assembled molecules' anchoring groups for surface defect passivation and dipole modulation in inverted perovskite solar cells

Xiaoyu Wang(王啸宇), Muhammad Faizan, Kun Zhou(周琨), Xinjiang Wang(王新江), Yuhao Fu(付钰豪), and Lijun Zhang(张立军)
Chin. Phys. B, 2024, 33 (**10**): 107303. DOI: 10.1088/1674-1056/ad711f

Polyhedral silver clusters as single molecule ammonia sensor based on charge transfer-induced plasmon enhancement

Jiu-Huan Chen(陈九环) and Xin-Lu Cheng(程新路)
Chin. Phys. B, 2023, 32 (**1**): 017302. DOI: 10.1088/1674-1056/ac6daf

First principles study on geometric and electronic properties of two-dimensional Nb_2CT_x MXenes

Guoliang Xu(徐国亮), Jing Wang(王晶), Xilin Zhang(张喜林), and Zongxian Yang(杨宗献)
Chin. Phys. B, 2022, 31 (**3**): 037304. DOI: 10.1088/1674-1056/ac322e

Effect of surface oxygen vacancy defects on the performance of ZnO quantum dots ultraviolet photodetector

Hongyu Ma(马宏宇), Kewei Liu(刘可为), Zhen Cheng(程祯), Zhiyao Zheng(郑智遥), Yinzhe Liu(刘寅哲), Peixuan Zhang(张培宣), Xing Chen(陈星), Deming Liu(刘德明), Lei Liu(刘雷), and Dezhen Shen(申德振)
Chin. Phys. B, 2021, 30 (**8**): 087303. DOI: 10.1088/1674-1056/ac0131

Enhanced thermoelectric properties in two-dimensional monolayer Si_2BN by adsorbing halogen atoms

Cheng-Wei Wu(吴成伟), Changqing Xiang(向长青), Hengyu Yang(杨恒玉), Wu-Xing Zhou(周五星), Guofeng Xie(谢国锋), Baoli Ou(欧宝立), and Dan Wu(伍丹)
Chin. Phys. B, 2021, 30 (**3**): 037304. DOI: 10.1088/1674-1056/abd163

High-throughput screening and evaluation of double-linker metal–organic frameworks for CO_2/H_2 adsorption and separation

Ji-Long Huang(黄纪龙)[1], Xiu-Ying Liu(刘秀英)[1,2,†], Hao Chen(陈浩)[1], Xiao-Dong Li(李晓东)[1,2], and Jing-Xin Yu(于景新)[1,2]

[1] *School of Physics, Henan University of Technology, Zhengzhou* 450001, *China*
[2] *R&D Center for Advanced Energy Materials, Henan University of Technology, Zhengzhou* 450001, *China*

(Received 8 September 2024; revised manuscript received 5 November 2024; accepted manuscript online 14 November 2024)

The capture of CO_2 from CO_2/H_2 gas mixtures in syngas is a crucial issue for hydrogen production from steam methane reforming in industry, as the presence of CO_2 directly affects the purity of H_2. A combination of a high-throughput screening method and grand canonical Monte Carlo simulation was utilized to evaluate and screen 1725 metal–organic frameworks (MOFs) in detail as a means of determining their adsorption performance for CO_2/H_2 gas mixtures. The adsorption and separation performance of double-linker MOFs was comprehensively evaluated using eight evaluation indicators, namely, the largest cavity diameter, accessible surface area, pore occupied accessible volume, porosity, adsorption selectivity, working capacity, adsorbent performance score and percent regeneration. Six optimal performance frameworks were screened to further study their single-component adsorption and binary competitive adsorption of CO_2/H_2 respectively. The CO_2 adsorption selectivity at different CO_2/H_2 feed ratios was also evaluated, which indicated their excellent adsorption and separation performance. The microscopic adsorption mechanisms for CO_2 and H_2 at the molecular level were investigated by analyzing the radial distribution function and density distribution. This study may provide directional guidance and reference for subsequent experiments on the adsorption and separation of CO_2/H_2.

Keywords: metal–organic framework, adsorption, separation, high-throughput screening, grand canonical Monte Carlo simulation

PACS: 73.22.–f, 36.40.–c, 71.15.Mb

DOI: 10.1088/1674-1056/ad925a **CSTR:** 32038.14.CPB.ad925a

1. Introduction

With the industrial development in modern society, the demand for fossil fuels is increasing, and the burning of fossil fuels leads to the intensification of the global greenhouse effect.[1] As CO_2 is the main culprit in the greenhouse effect, how to capture it has become a scientific challenge. CO_2 capture in syngas from hydrogen produced by the steam methane reforming process has received widespread attention. Syngas is mainly composed of CO_2 and H_2. Separating CO_2 from H_2 in syngas to obtain high-purity H_2 is the key to industrial production of H_2 from methane.[2–4] Organic amine scrubbing to separate CO_2/H_2 mixtures is a common process used in industry, but amine regeneration is an energy-intensive process.[5–7] Adsorption and separation of CO_2/H_2 gas mixtures by porous materials, which is both energy efficient and environmentally friendly, is expected to replace conventional methods of gas separation in industry.

As a commonly used porous material, metal–organic frameworks (MOFs) have the advantages of diversified structure, large porosity and adjustable pore size[8,9] and are extensively applied in gas adsorption and separation,[10–13] catalysis,[14,15] sensors,[16–18] drug delivery[19–21] and energy storage.[22,23] MOFs have been widely explored for CO_2 capture and separation of CO_2-containing gas mixtures. MOFs are built by combining metal atoms or clusters and organic ligands, so an infinite number of MOFs can theoretically be synthesized. MOF databases with a total number of MOFs approaching a million have been created in recent years, which facilitates computational screening for superior materials. The traditional exploration method is to experimentally synthesize these materials for analysis, but this is time and resource intensive. High-throughput screening methods are widely used to compute a large number of structures at the same time for analyzing material performance due to their lower time and cost.[24] Replacing traditional experimental synthesis and testing methods with a high-throughput screening method may improve the efficiency of screening high-performance materials. Qiao *et al.*[25] simulated 4764 MOFs for CO_2 capture in CO_2/CH_4 and CO_2/N_2 using a high-throughput screening method, and screened 30 lanthanide metal MOFs with the best separation performance. Avci *et al.*[26] systematically investigated 54 808 MOFs from the Cambridge data by a high-throughput screening method for the adsorption and separation of a CO_2/H_2 binary mixture and identified the 20 most promising MOFs. Li *et al.*[27] selected 5732 MOFs with open Cu sites from the TOBACCO-MOF database for high-throughput

[†]Corresponding author. E-mail: liuxiuyingzx@126.com

© 2025 Chinese Physical Society and IOP Publishing Ltd. All rights, including for text and data mining, AI training, and similar technologies, are reserved.

screening and their results showed that 1,2,4,5-tetrazine has good adsorption and separation performance for CO_2/H_2. These research works suggest that MOFs have promising applications in CO_2/H_2 adsorption and separation, and the performance of more MOFs awaits exploration. Ryu and Kim[28] developed a database of 1725 double-linker MOFs with the advantages of larger pore size and porosity than most experimental MOFs, and investigated their adsorption performance for H_2 molecules. However, the double-linker MOFs did not exhibit a promising adsorption capacity for H_2, which is anticipated to confer potential advantages in the adsorption and separation of CO_2/H_2 gas mixtures. The adsorption and separation performance of double-linker MOFs for CO_2/H_2 gas mixtures has not yet been investigated, and more adsorption and separation mechanisms remain to be revealed.

Therefore, the adsorption and separation performances of 1725 double-linker MOFs for a CO_2/H_2 mixed system were comprehensively investigated using a combination of high-throughput screening and grand canonical Monte Carlo (GCMC) simulation. Previous high-throughput screening endeavors have predominantly relied on the criterion of selectivity as their foundation. In this study, the adsorption and separation performance of the 1725 double-linker MOF materials was comprehensively evaluated using eight screened descriptors, including the largest cavity diameter (LCD), accessible surface area (ASA), pore occupied accessible volume (POAV), porosity, adsorption selectivity, working capacity, adsorbent performance score and percent regeneration (R%). After a series of rigorous screenings based on these descriptors, six promising frameworks were identified, which demonstrated optimal efficiency for the separation of CO_2 and H_2. Subsequently, a comprehensive assessment was performed to analyze the adsorption and separation performances of a CO_2/H_2 single-component and binary mixed-component for CO_2/H_2 molecules. The microscopic adsorption mechanisms for CO_2 and H_2 were revealed by analyzing the radial distribution function (RDF) and the density distribution at the molecular level. This research will provide some theoretical guidance for CO_2 trapping and H_2 purification, and it also provides a novel idea for the screening process of MOFs in adsorption and separation.

2. Materials and methods

2.1. High-throughput calculation

A high-throughput screening method based on molecular simulation is adopted, and the screening process is shown in Fig. 1. Firstly, the geometric structures of 1725 double-linker MOFs[28] were optimized, then the LCD, ASA and POAV of these frameworks were calculated by Zeo ++ software using helium as the probe molecule (kinetic radius of 1.3 Å).[29] The porosity was calculated by Raspa 2.0 software. Finally, 92 frameworks with ASA equal to 0 and a non-zero net charge were excluded. For the 1633 screened frameworks, the adsorption isotherms of pure CO_2 and H_2 and the adsorption selectivity of mixed CO_2/H_2 at 298 K and 1 bar were calculated by GCMC simulation. Finally, according to the relationship between the eight descriptors mentioned above and the adsorption separation performance, six top-performing frameworks for CO_2 were screened and their adsorption and separation performances for CO_2 and H_2 were further investigated.

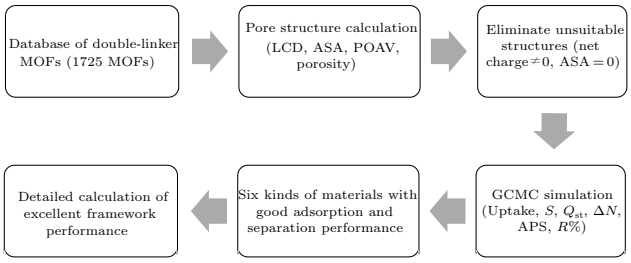


Fig. 1. High-throughput screening process.

2.2. Force field

The Dreiding force field[30] excels in modeling organic small molecules, macromolecules and main-group elements. The universal force field (UFF)[31] has a wider applicability, covering all the elements in the periodic table. Therefore, the UFF and Dreiding force fields were used for metallic and non-metallic elements in this study, respectively. Combined use of these two force fields has been successfully applied and validated in previous adsorption studies of other MOFs.[32–34] In addition, this study aims to identify the materials with excellent performance from many MOF materials, focusing on the ranking trend of material properties rather than the absolute value of the performance data, so the accuracy of the force field has little influence on the results presented in this paper.

Both CO_2 and H_2 molecules are treated as a rigid three-point model. For the H_2 molecule, a pseudopotential atom is introduced at the center to simulate the experimental quadrupole moment action. Their potential energy parameters are obtained from the TraPPE force field,[35] which well describes the interaction between the framework and the gas molecules. The detailed potential energy parameters are given in Table 1.

Table 1. Force field parameters of CO_2 and H_2.

	Atom	ε/k_B (K)	σ (Å)	q/e
CO_2	C	27.0	2.80	0.70
	O	79.0	3.05	−0.35
H_2	H	36.7	2.958	0.468
	com	0	0	−0.936

2.3. Structure of the six optimal performance frameworks

Structural diagrams of the six optimal performance MOFs are depicted in Fig. 2, while the pore structure data

for the frameworks can be found in Table 2. The pore size of the frameworks is between 5.487 Å and 7.816 Å classified as microporous material. d_bto+N536+E150 and d_hcb+N481+E150 are triclinic structures, while d_cdt+N548+E80, d_cdt+N406+E11494891_, d_clh+N536+E150 and d_dia-g+N536+E150 are tetragonal structures. d_bto+N536+E150, d_cdt+N548+E80, d_clh+N536+E150 and d_dia-g+N536+E150 have an irregular pore structure. d_cdt+N406+E11494891_ and d_hcb+N481+E150 have approximately elliptical pore structures. They all contain C, H and O, among which d_bto+N536+E150, d_cdt+N406+E11494891_ and d_clh+N536+E150 also contain Cr, and d_cdt+N406+E11494891_ also contain N, S and Mg. d_cdt+N548+E80 also contains N and Mn and d_hcb+N481+E150 also contains Fe.

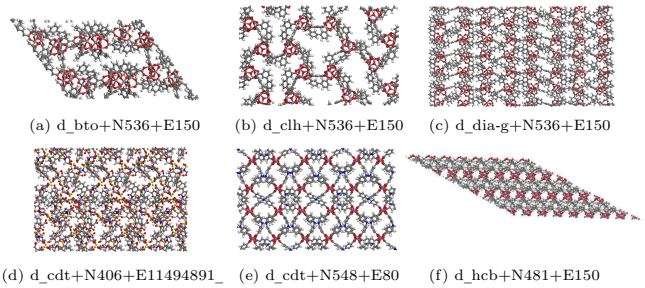


Fig. 2. Structure of double-linker MOFs: (a) d_bto+N536+E150, (b) d_clh+N536+E150, (c) d_dia-g+N536+E150, (d) d_cdt+N406+E11494891_, (e) d_cdt+N548+E80 and (f) d_hcb+N481+E150.

Table 2. Structural parameters of MOFs d_bto+N536+E150, d_cdt+N548+E80, d_cdt+N406+E11494891_, d_clh+N536+E150, d_dia-g+N536+E150 and d_hcb+N481+E150.

MOF	LCD (Å)	ASA (m^2/g^{-1})	POAV ($cm^3 \cdot g^{-1}$)	Porosity
d_bto+N536+E150	7.440	2000.41	0.583	0.463
d_cdt+N548+E80	7.249	1321.08	0.454	0.339
d_cdt+N406+E11494891_	5.487	1531.82	0.470	0.364
d_clh+N536+E150	7.816	2386.41	0.675	0.544
d_dia-g+N536+E150	6.715	1976.55	0.562	0.469
d_hcb+N481+E150	6.915	1421.61	0.478	0.417

2.4. GCMC simulation details

The interaction between adsorbates and adsorbent molecules is often represented by the Lennard–Jones (L–J) potential, which can be represented by[36–38]

$$U_{ij} = 4\varepsilon_{ij}\left[\left(\frac{\sigma_{ij}}{r_{ij}}\right)^{12} - \left(\frac{\sigma_{ij}}{r_{ij}}\right)^{6}\right] + \frac{q_i q_j}{4\pi\varepsilon_0 r_{ij}}, \tag{1}$$

where the potential energy of the interacting atoms i and j is expressed as U_{ij}. The distance between the atoms is r_{ij}. The depth and diameter of the L–J potential trap are ε_{ij} and σ_{ij}, respectively. The corresponding partial charges are q_i and q_j, respectively, and the dielectric constant is ε_0. The cross interaction between different atoms is calculated by the Lorentz–Berthelot (L–B) mixing rule[39–41]

$$\sigma_{ij} = \frac{1}{2}(\sigma_{ii} + \sigma_{jj}), \tag{2}$$

$$\varepsilon_{ij} = \sqrt{\varepsilon_{ii}\varepsilon_{jj}}. \tag{3}$$

All GCMC simulations are performed using RASPA 2.0 software.[42,43] The material is regarded as a rigid framework, and the truncation radius of the interaction between adsorbates and adsorbent molecules is set to 12.0 Å in order to ensure that the length of the unit cell of the frameworks is no less than twice the truncation radius.[44] For the adsorption process, the frameworks are calculated using supercells. 2×10^4 cycles are set during the simulation, of which 1×10^4 cycles are used to calculate the system equilibrium and the other 1×10^4 cycles are used to calculate the average of the results to ensure the accuracy of the simulation process.

In the adsorption process, the isosteric heat of adsorption (Q_{st}) is calculated by

$$Q_{st} = -\Delta H = -U_{hg} + U_h + U_g + RT, \tag{4}$$

where U_{hg} represents the interaction between subject and guest, U_h and U_g represent the subject interaction and object interaction, respectively. R and T are the universal gas constant and the temperature of system, respectively. Both U_h and U_g are 0 as both the frameworks and gas molecules are considered rigid.[45,46]

Adsorption selectivity is one of the parameters for evaluating the separation performance of the framework in the binary adsorption process of mixed gases, and is calculated by[47]

$$S_{CO_2/H_2} = \frac{x_{CO_2} y_{H_2}}{x_{H_2} y_{CO_2}}, \tag{5}$$

where x_{CO_2} and x_{H_2} represent the absolute adsorption uptakes of CO_2 and H_2, respectively. y_{CO_2} and y_{H_2} are the partial pressures of CO_2 and H_2 in the gas mixture, respectively; a large value of S indicates an excellent separation performance of the porous material.

In addition, the working capacity (ΔN), percent regeneration ($R\%$) and adsorbent performance score (APS) of the frameworks are calculated by

$$\Delta N = N_{ads,CO_2} - N_{des,CO_2}, \tag{6}$$

$$R\% = \frac{\Delta N_{CO_2}}{N_{ads,CO_2}} \times 100\%, \tag{7}$$

$$\text{APS} = \Delta N \times S, \tag{8}$$

where N_{ads} and N_{des} are the gas absorption rates under adsorption and desorption conditions, respectively. During the simulation, the adsorption (desorption) pressure is set to 1 bar (0.1 bar).[26,48]

3. Results and discussion

3.1. Structural characterization of MOF frameworks

After excluding ASA and non-zero net charge structures, the GCMC simulation was performed for 1633 qualified structures, and the adsorption performance data were obtained at 298 K and 1 bar. Four key geometrical descriptors are discussed, including LCD, ASA, POAV and porosity. Furthermore, the discussion also delves into the inherent relationship between the energy descriptor Q_{st} and its impact on adsorption performance. Figure 3 shows the relationship between the geometric parameters of these structures and the CO_2 adsorption performance. Figure 3(a) shows the excellent uptake for the framework with LCD distribution in the range of 5–15 Å, which indicates that the microporous material favors CO_2 adsorption. Figure 3(b) shows that the uptake is large for the frameworks with a POAV distribution in the range of 0.23–2 $cm^3 \cdot g^{-1}$. As seen in Figs. 3(c) and 3(d), the values of ASA and porosity with excellent uptake are mainly distributed in the intervals of 1400–2500 $m^2 \cdot g^{-1}$ and 0.34–0.55, respectively. The uptake increases with increase in ASA, reaching a maximum at an ASA of about 2000 $m^2 \cdot g^{-1}$, then it decreases with increase in ASA. Overall, the CO_2 uptake of the studied double-linker MOFs reaches its maximum value when the LCD is close to 7 Å, the ASA is about 1500 $m^2 \cdot g^{-1}$, the POAV is about 0.5 $cm^3 \cdot g^{-1}$ and the porosity is about 0.5. In addition, the Q_{st} of CO_2 is primarily concentrated within the range 3–24 $kJ \cdot mol^{-1}$, and its distribution is positively correlated with the uptake.

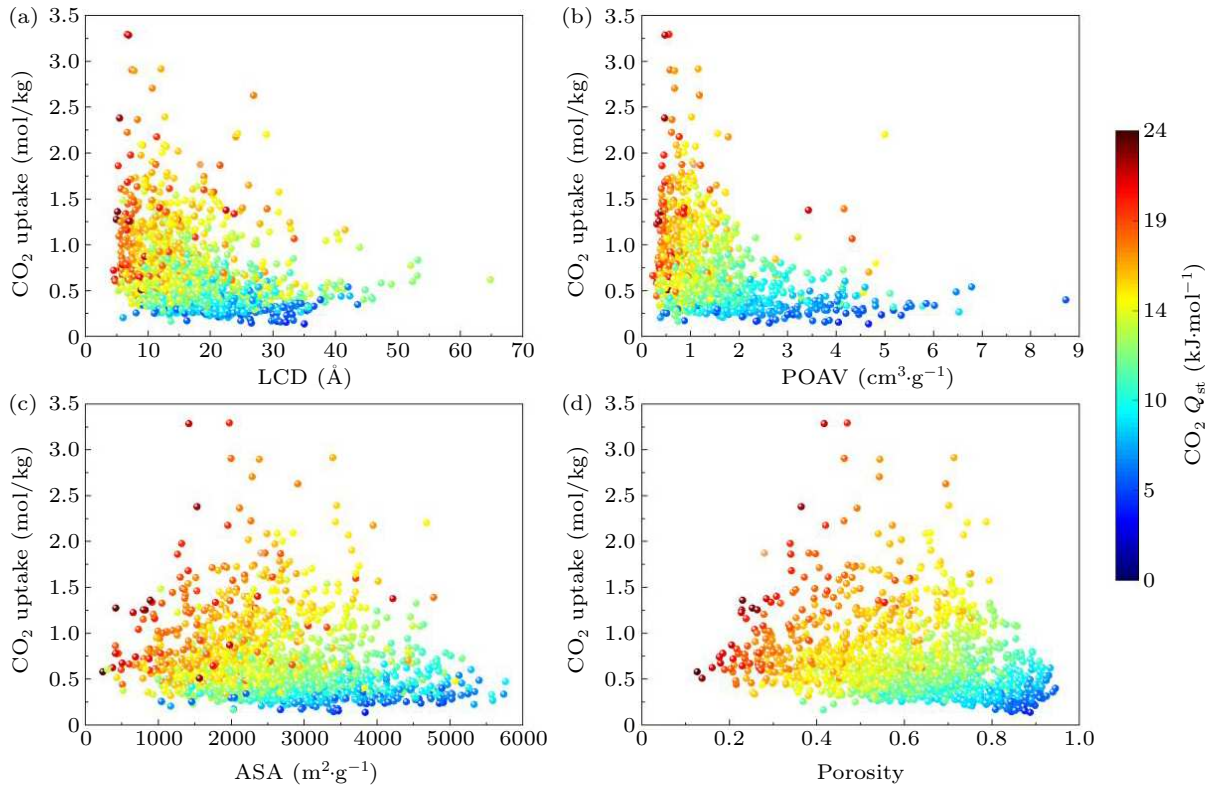


Fig. 3. The relationship between uptake of double-linker MOFs and LCD (a), POAV (b), ASA (c) and porosity (d).

Figure 4 shows the relationship between the adsorption selectivity of the CO_2/H_2 mixed system on the framework and four structural descriptors of the frameworks. As seen in Figs. 4(a) and 4(b), when the LCD of the frameworks is about 7 Å and the POAV is close to 0.5 $cm^3 \cdot g^{-1}$, the adsorption selectivity of CO_2 has its highest value. This trend is consistent with the changes in CO_2 adsorption shown in Figs. 3(a) and 3(b). At the same time, figures 4(c) and 4(d) demonstrate that when the ASA is close to 700 $m^2 \cdot g^{-1}$ and porosity is about 0.25, the adsorption selectivity of CO_2 also reaches its maximum.

Figure 5(a) depicts the relationship between LCD and POAV in the frameworks. As the LCD increases, the POAV increases accordingly. This trend is similar to the relationship between the uptake and adsorption selectivity of CO_2 for LCD and POAV shown in Figs. 3 and 4. Figure 5(b) depicts the correlation between the Q_{st} of CO_2 and adsorption selectivity. It can be observed that there is a positive correlation between the Q_{st} of CO_2 and the adsorption selectivity, especially when the value of Q_{st} exceeds 16 $kJ \cdot mol^{-1}$ and the CO_2 adsorption selectivity undergoes a substantial augmentation. Figure 5(c) shows that the adsorption selectivity of CO_2 and the adsorption capacity of MOFs are not directly related. Some MOFs with higher selectivity for CO_2 may not have a higher adsorption capacity. This is because the adsorption selectivity of CO_2 is defined as in Eq. (5) in Subsection 2.5. This formula shows

that the reason why the selectivity is high is mainly because the difference in adsorption capacity of CO_2 and H_2 molecules in MOFs is relatively large. For example, although the adsorption capacity of CO_2 is not high, the adsorption capacity of H_2 is even lower, resulting in a high selectivity and making it more favorable for the separation of these two molecules. Although the adsorption capacity of MOFs on CO_2 molecules may be very high, the H_2 adsorption capacity of MOFs is also relatively large at the same time, resulting in the adsorption capacity of the two molecules being relatively close; thus the selectivity is relatively low, which is not favorable for their separation.

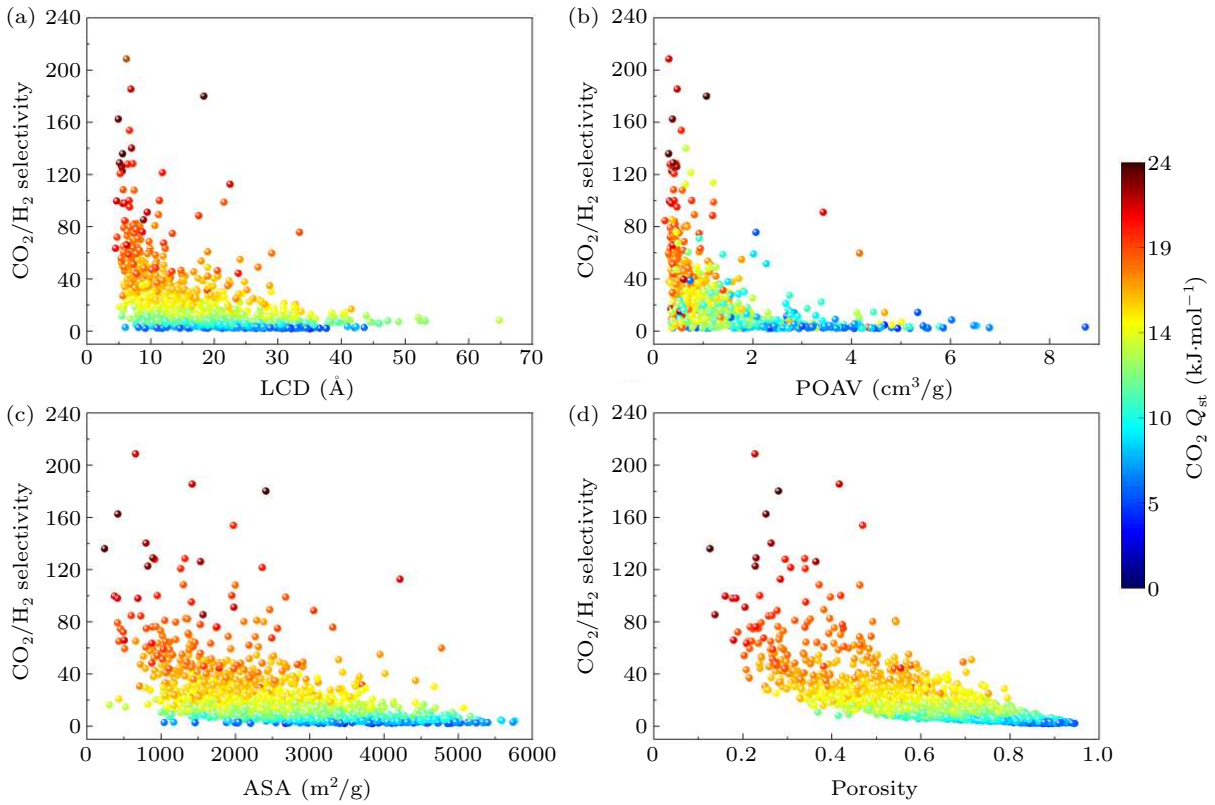


Fig. 4. The relationship between the CO_2 selectivity of double-linker MOFs and LCD (a), POAV (b), ASA (c) and porosity (d).

Based on this, the ΔN, $R\%$ and APS of the framework were calculated, and the relationships are shown in Fig. 6. Figure 6(a) shows the relationship between ΔN and the adsorption selectivity of CO_2. This relationship has the same trend as that in Fig. 5(b), and most of the frameworks in the figure have a 'blue' APS, which indicates that the APS of these frameworks is smaller. Our aim is to screen the frameworks with higher APS, and the brown–red frameworks near the upper right corner are the preferred frameworks. Figure 6(b) shows the relationship between the adsorption selectivity of CO_2 and $R\%$. We can see that the $R\%$ of the frameworks is negatively correlated with the adsorption selectivity of CO_2. As the MOFs with high CO_2/H_2 selectivity strongly adsorb CO_2 molecules rather than H_2 molecules, the desorption of CO_2 becomes difficult, resulting in a low working capacity (ΔN) and low percent regeneration ($R\%$). Although the $R\%$ of most of the frameworks is above 80%, the selectivity of these frameworks is less than 100. Figure 6(c) shows that the $R\%$ of the frameworks gradually decreases with increase in APS, which is the same trend as that in Fig. 6(b). Based on the trade-off between the two parameters, six top-performing frameworks, d_bto+N536+E150, d_clh+N536+E150, d_dia-g+N536+E150, d_hcb+N481+E150, d_cdt+N548+E80 and d_cdt+N406+E11494891_, which are labeled by the pentagram in Fig. 6(c), were screened out with the condition of APS $>$ 200 and $R\% > 80\%$. The ΔN, CO_2/H_2 selectivity, APS and $R\%$ data for the six top-performing frameworks are listed in Table 3.

Table 3. The ΔN, CO_2/H_2 selectivity, APS and $R\%$ data for the six top-performing frameworks.

Framework	ΔN ($mol \cdot kg^{-1}$)	$S(CO_2/H_2)$	APS ($mol \cdot kg^{-1}$)	$R\%$
d_bto+N536+E150	2.425	107.990	261.889	83.46
d_cdt+N548+E80	1.608	128.341	206.419	81.32
d_cdt+N406+E11494891_	2.016	125.941	253.911	84.70
d_clh+N536+E150	2.521	79.768	201.097	87.07
d_dia-g+N536+E150	2.663	153.817	409.680	80.91
d_hcb+N481+E150	2.732	185.469	506.705	83.20

Table 4 presents the CO_2 selectivity of some reported MOFs and the MOFs in this study to compare the CO_2 separation performance of double-linker MOFs and other MOFs

in CO_2/H_2 mixed systems. It is evident that the double-linker MOFs have excellent CO_2 selectivity at 298 K and 10 bar, similar to the other MOFs. It is noted that the CO_2 selectivity of double-linker MOFs in this study is much higher than that of Co-btec SC at 298 K and 1 bar, which suggests that double-linker MOFs are a potential material for CO_2/H_2 separation.

Table 4. Comparison of the selectivity of CO_2/H_2 in MOFs in this study with the reported results in Refs. [27,49].

Materials	Temperature (K)	Pressure (bar)	CO_2 selectivity	Reference
MOF-4641	298	10	166.680	[27]
MOF-8595	298	10	80.520	[27]
MOF-7159	298	10	209.870	[27]
MOF-4867	298	10	155.600	[27]
Co-btec SC	298	1	18.790	[49]
d_bto+N536+E150	298	10 (1)	91.579 (107.990)	this study
d_cdt+N548+E80	298	10 (1)	100.659 (128.341)	this study
d_cdt+N406+E11494891_	298	10 (1)	88.100 (125.941)	this study
d_clh+N536+E150	298	10 (1)	76.876 (79.768)	this study
d_dia-g+N536+E150	298	10 (1)	106.569 (153.817)	this study
d_hcb+N481+E150	298	10 (1)	178.311 (185.469)	this study

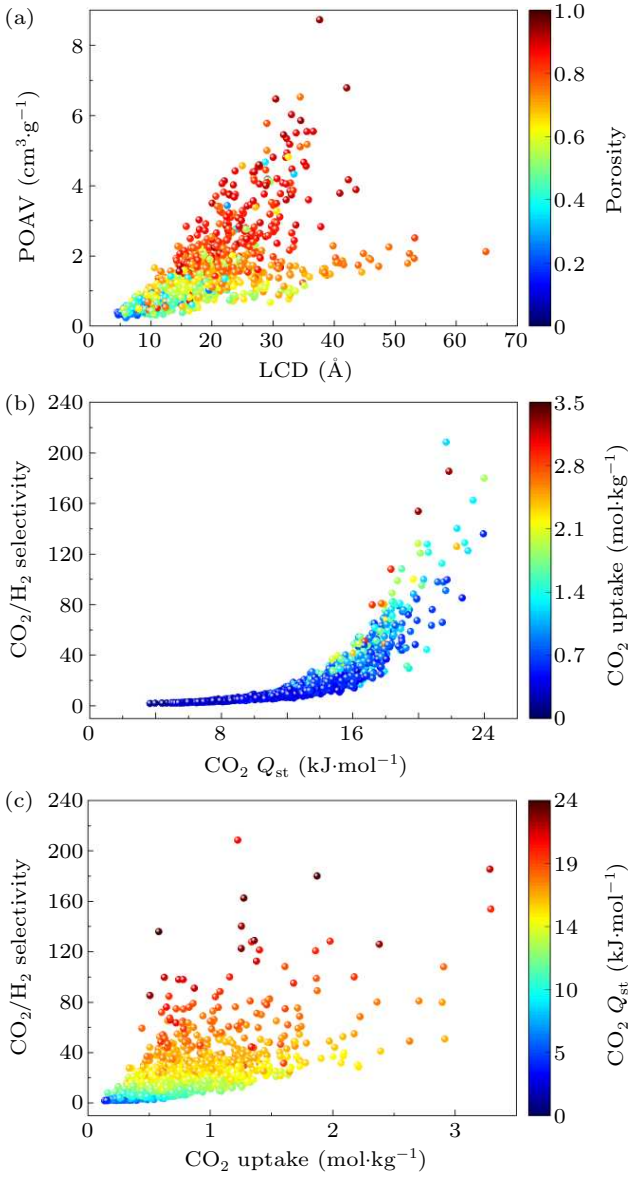


Fig. 5. (a) Correlation between the LCD and POAV of double-linker MOFs. (b) Correlation between CO_2 Q_{st} and CO_2 selectivity. (c) Correlation between CO_2 uptake and CO_2 selectivity of double-linker MOFs.

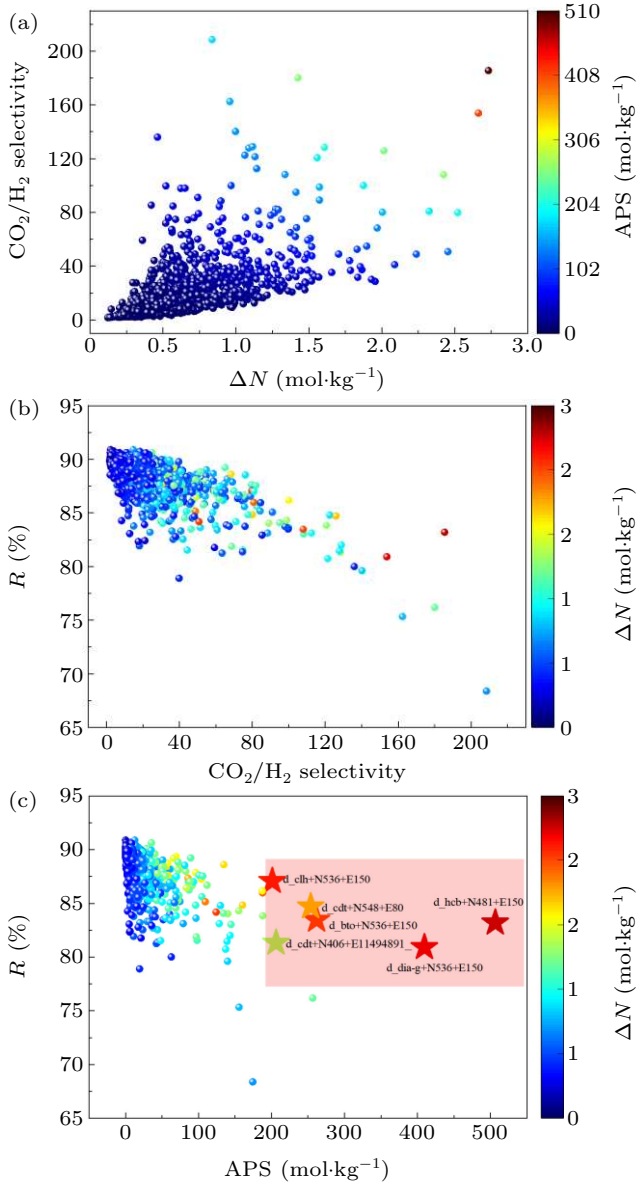


Fig. 6. (a) Correlation between CO_2 ΔN and CO_2 selectivity. (b) Correlation between CO_2 selectivity and R%. (c) Correlation between APS and R% of the frameworks.

3.2. Single-component adsorption of CO_2 in double-linker MOFs with optimal performance

The CO_2 adsorption isotherms of six top-performing double-linker MOFs were calculated using the GCMC method at a temperature of 298 K and 1–10 bar pressure; as shown in Fig. 7(a) they are typical Langmuir curves. At a pressure of 10 bar, the order of CO_2 uptake of the frameworks is: d_clh+N536+E150 > d_bto+N536+E150 > d_dia-g+N536+E150 > d_hcb+N481+E150 > d_cdt+N548+E80 > d_cdt+N406+E11494891_. The CO_2 uptake of d_hcb+N481+E150 increases the fastest at 0–1 bar, but when the pressure continues to increase to 10 bar the uptake of d_hcb+N481+E150 only reaches 5.948 mol·kg^{-1}, which is a medium value. The uptake of d_clh+N536+E150, which has a slower growth rate at 0–1 bar, is the highest (8.394 mol·kg^{-1}) at 10 bar. Figure 7(b) shows the relationship between Q_{st} and the uptake of the frameworks. The Q_{st} of the frameworks slightly decreases with increase in uptake, due to the increase in the number of CO_2 molecules in the framework making the spacing between the CO_2 molecules smaller and the repulsive forces increase. It is noteworthy that while the initial Q_{st} of d_hcb+N481+E150 is superior to that of the other five frameworks, its uptake at 10 bar is not the highest. This suggests that the pore structure of the framework exerts a more significant influence on adsorption than the energy effect of the framework itself.

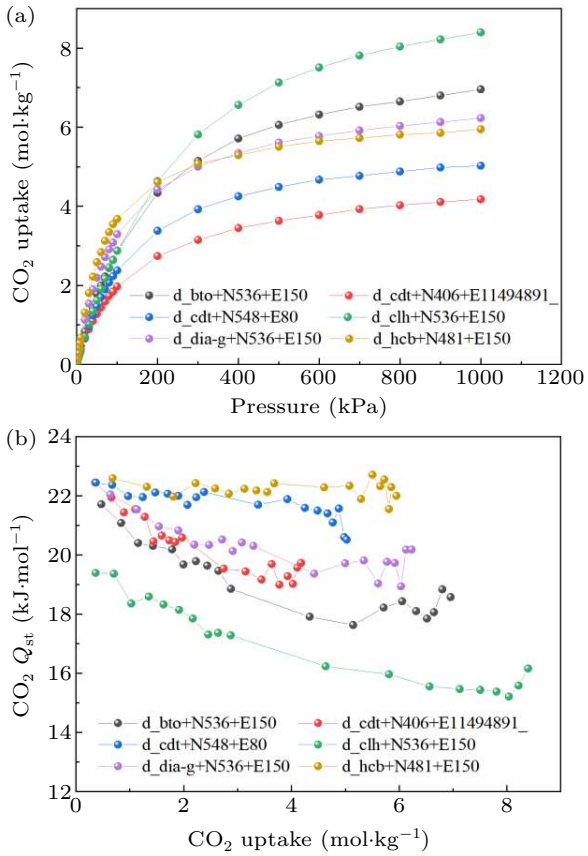


Fig. 7. The uptake (a) and Q_{st} (b) of CO_2 in double-linker MOFs at 298 K and 1–10 bar.

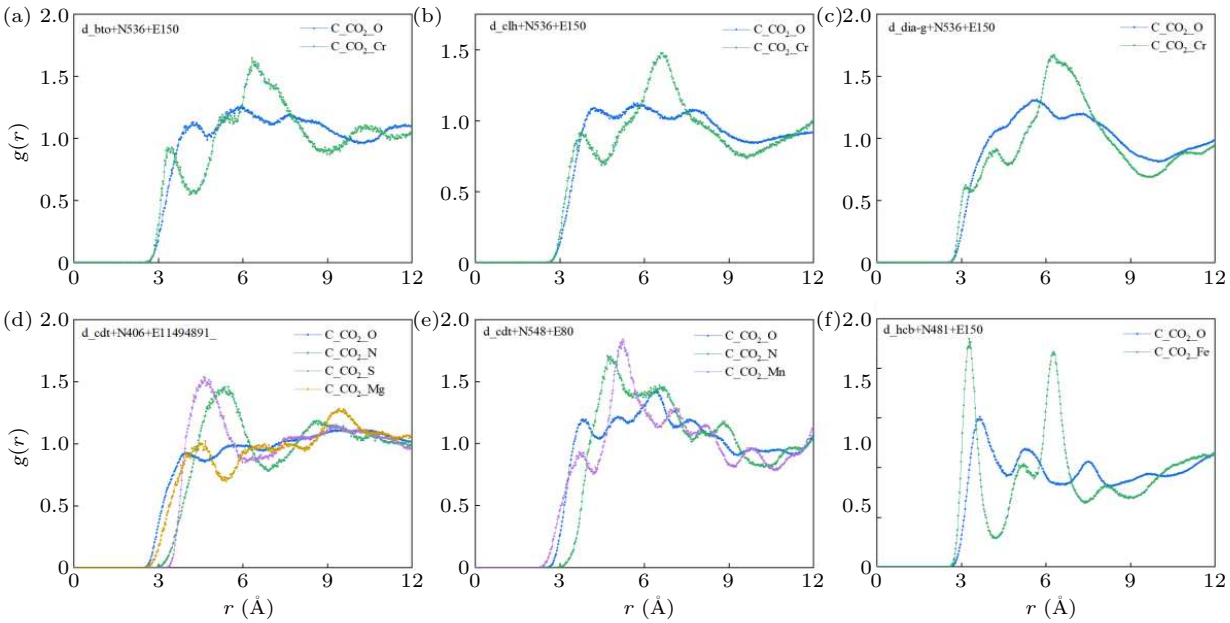


Fig. 8. The RDF between framework atoms and CO_2 molecules of (a) d_bto+N536+E150, (b) d_clh+N536+E150, (c) d_dia-g+N536+E150, (d) d_cdt+N406+E11494891_, (e) d_cdt+N548+E80 and (f) d_hcb+N481+E150 at 298 K and 1 bar.

Figure 8 illustrates the RDF between each atom in the frameworks and the C atom in CO_2 (C_CO_2) under the conditions of 298 K and 1 bar. The RDFs between C_CO_2 and C and H atoms in the frameworks are ignored, highlighting the distribution of enriched electrons such as metal atoms. The first peaks of d_bto+N536+E150, d_clh+N536+E150 and d_dia-g+N536+E150 are C_CO_2_Cr atomic pairs, and the strongest peaks are also C_CO_2_Cr atomic pairs (in Figs. 8(a)–8(c)), indicating that CO_2 in these three frameworks is mainly adsorbed near Cr atoms. This corresponds to the density distri-

bution of CO_2 in Figs. 9(a)–9(c). The first and strongest peaks of d_cdt+N406+E11494891_ are C_CO_2_S and C_CO_2_N atomic pairs, respectively (Fig. 8(d)). The first peak of d_cdt+N548+E80 is C_CO_2_Mn and C_CO_2_O atomic pairs, and the strongest peak is C_CO_2_Mn atomic pairs (Fig. 8(e)). The first peak of d_hcb+N481+E150 is also the strongest peak, which is a C_CO_2_Fe atom pair (Fig. 8(f)). As depicted in Fig. 9(d), CO_2 molecules are mainly distributed irregularly in holes close to S and N atoms. In Fig. 9(e), the largest number of CO_2 molecules are found in the middle of the line between the nearest two Mn atoms. Figure 9(f) illustrates that CO_2 molecules are most distributed in the middle of the line between two adjacent Fe atoms. The entire density distribution corresponds to the RDF.

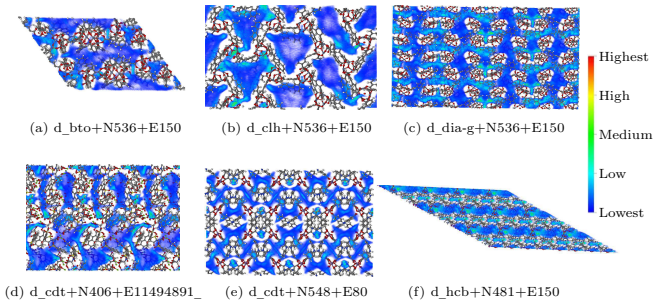


Fig. 9. Density distribution of CO_2 in double-linker MOFs: (a) d_bto+N536+E150, (b) d_clh+N536+E150, (c) d_dia-g+N536+E150, (d) d_cdt+N406+E11494891_, (e) d_cdt+N548+E80 and (f) d_hcb+N481+E150 at 298 K and 1 bar.

3.3. Single-component adsorption of H_2 in double-linker MOFs with optimal performance

The adsorption isotherms of H_2 in the six top-performing double-linker MOFs at 298 K and 1–10 bar were calculated and are shown in Fig. 10(a). The adsorption curve of H_2 in the framework is basically a straight line. At a pressure of 10 bar, the order of H_2 uptake of the framework is as

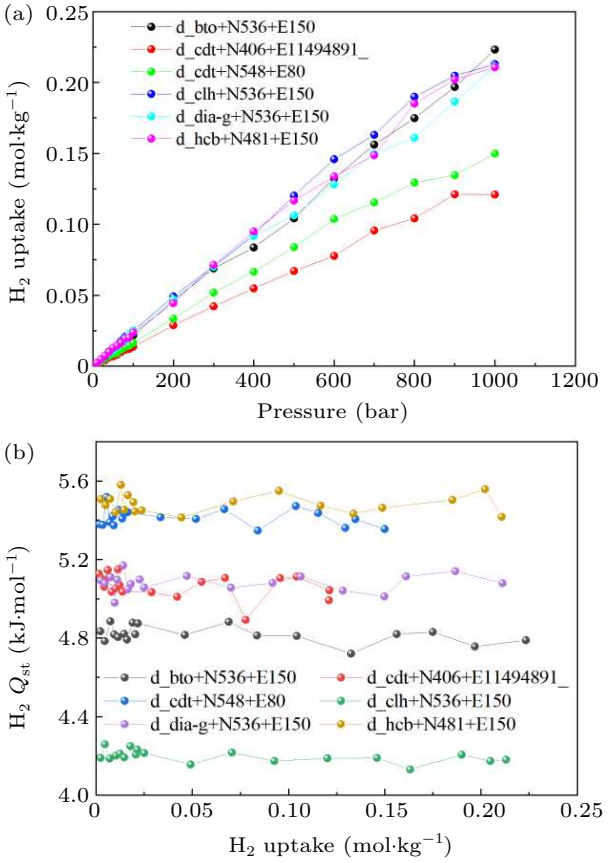


Fig. 10. The uptake (a) and Q_{st} (b) of H_2 in double-linker MOFs at 298 K and 1–10 bar.

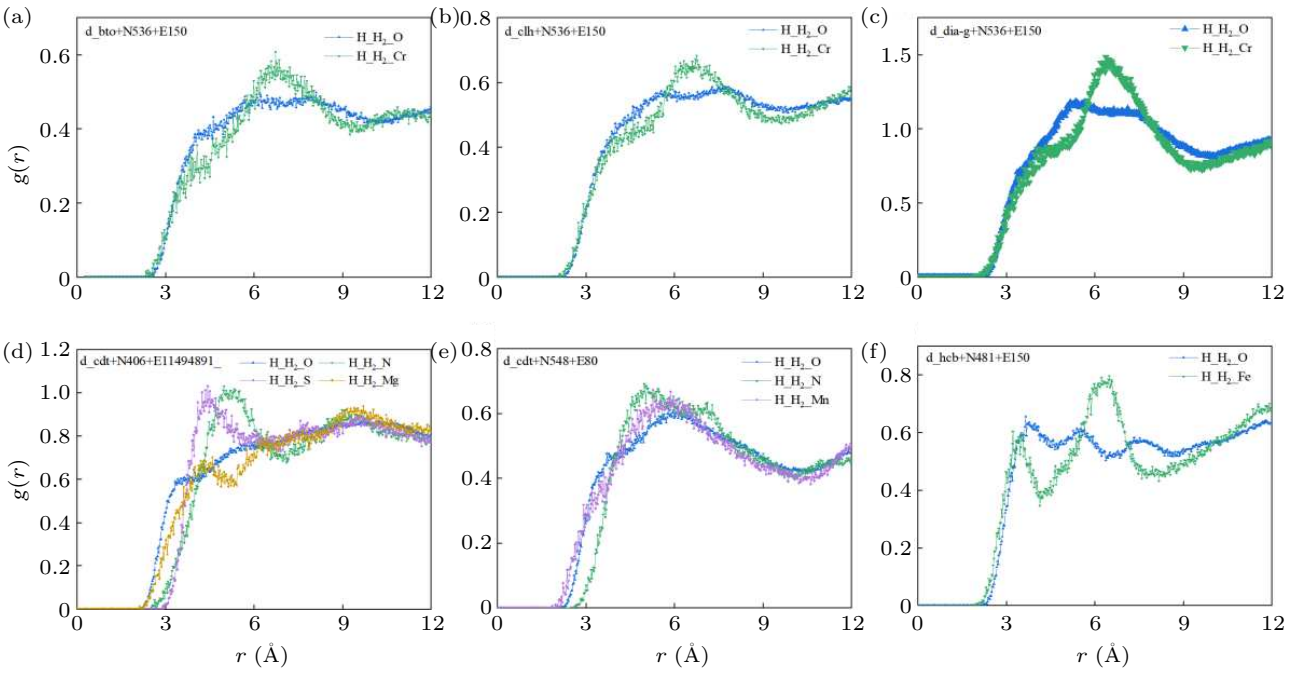


Fig. 11. The RDF between framework atoms and CO_2 molecules of (a) d_bto+N536+E150, (b) d_clh+N536+E150, (c) d_dia-g+N536+E150, (d) d_cdt+N406+E11494891_, (e) d_cdt+N548+E80 and (f) d_hcb+N481+E150 at 298 K and 1 bar.

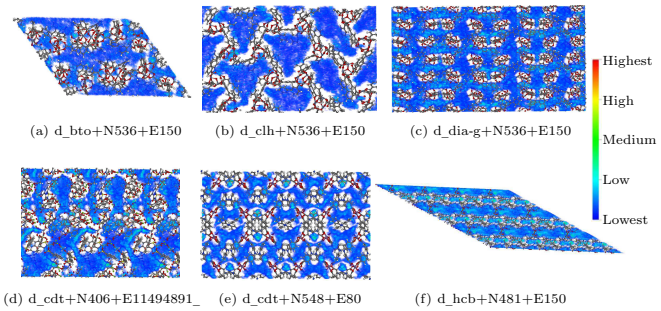


Fig. 12. Density distribution of CO_2 in double-linker MOFs: (a) d_bto+N536+E150, (b) d_clh+N536+E150, (c) d_dia-g+N536+E150, (d) d_cdt+N406+E11494891_, (e) d_cdt+N548+E80 and (f) d_hcb+N481+E150 at 298 K and 1 bar.

follows: d_bto+N536+E150 > d_clh+N536+E150 > d_dia-g+N536+E150 > d_hcb+N481+E150 > d_cdt+N548+E80 > d_cdt+N406+E11494891_. This order is basically consistent with the order of CO_2 uptake. The H_2 uptake of the six frameworks is in the range 0.121–0.223 mol·kg^{-1}, which is overall smaller than the smallest CO_2 uptake (4.178 mol·kg^{-1}). Figure 10(b) shows the Q_{st} curve of the framework. The Q_{st} of the six double-linker MOFs basically does not change with the change in uptake and always remains near a fixed value. The highest Q_{st}, of d_hcb+N481+E150, is only 5.579 kJ·mol^{-1}, and the H_2 Q_{st} of all frameworks is lower than that of CO_2, which is consistent with the trend that the H_2 uptake is lower than that of CO_2.

Figures 11 and 12 show the RDF and density distribution between each atom in the frameworks and the H atom (H_H_2) in H_2 at a temperature of 298 K and a pressure of 1 bar. The RDF of H_2 is similar to that of CO_2, and the distribution density is basically the same as that of CO_2 adsorption. The difference is that H_2 occupies a larger space than CO_2, which may be because the kinetic diameter of H_2 molecules is smaller than that of CO_2 molecules.

3.4. Binary competitive adsorption of CO_2/H_2 in double-linker MOFs with optimal performance

The adsorption selectivity of double-linker MOFs for CO_2/H_2 binary mixed systems with different feed ratios at a temperature of 298 K and pressure of 1–10 bar was investigated; the results are shown in Fig. 13. The adsorption selectivity of CO_2 in the same framework follows the same trend with increasing pressure, independent of the CO_2/H_2 feed ratio. The CO_2 selectivity of d_hcb+N481+E150 and d_clh+N536+E150 increases with increase in pressure, while that of d_dia-g+N536+E150 and d_cdt+N406+E11494891_ decreases with increasing pressure. The CO_2 selectivity of d_bto+N536+E150 and d_cdt+N548+E80 remains almost unchanged. Therefore, it is concluded that the separation performance of the framework for the CO_2/H_2 binary mixed system is affected by the CO_2 concentration, with a higher CO_2 concentration leading to better separation.

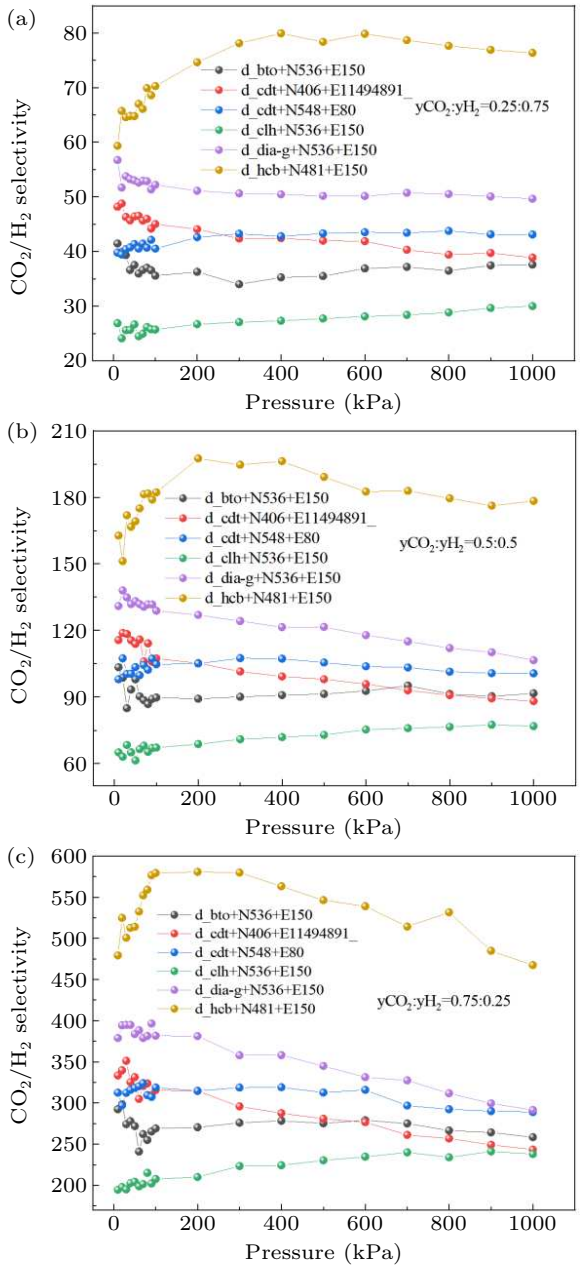


Fig. 13. CO_2 adsorption selectivity in double-linker MOFs at different CO_2/H_2 feed ratios: (a) $y_{CO_2} : y_{H_2} = 0.25 : 0.75$, (b) $y_{CO_2} : y_{H_2} = 0.5 : 0.5$, (c) $y_{CO_2} : y_{H_2} = 0.75 : 0.25$.

4. Conclusion

The adsorption and separation performance of 1725 double-linker MOFs was comprehensively investigated using a combination of GCMC simulations and high-throughput calculations. Eight screened descriptors, including largest cavity diameter, accessible surface area, pore occupied accessible volume, porosity, adsorption selectivity, working capacity, adsorbent performance score and percent regeneration were used to evaluate the CO_2/H_2 adsorption and separation performance of the frameworks. Based on the comprehensive evaluation of these eight descriptors, six best candidate frameworks for CO_2/H_2 separation were screened: d_bto+N536+E150, d_clh+N536+E150, d_dia-

g+N536+E150, d_hcb+N481+E150, d_cdt+N548+E80 and d_ cdt+N406+E11494891_. Their excellent adsorption and separation performances were verified by analyzing the single-component adsorption and binary competitive adsorption of CO_2/H_2. The finding that the selectivity of CO_2 is positively correlated with the CO_2 concentration in the mixed system expands the application scenario of the framework for separation of CO_2 in mixed CO_2/H_2 systems with different ratios. The microscopic adsorption mechanism of the frameworks was analyzed at the molecular level by means of the radial distribution functions and density distribution, and the results showed that the geometry of the frameworks significantly affects the adsorption performance. This study will be of assistance for subsequent studies of MOFs in gas adsorption and separation.

Acknowledgments

Project supported by the National Natural Science Foundation of China (Grant Nos. 11304079, 11404094, and 11504088) and Science and Technology Research Project of Henan Science and Technology Department (Grant No. 182102410076).

References

[1] Zhang M M, Zhang F, Wu Q, Huang X, Yan W, Zhao C M, Chen W, Yang Z H, Wang Y H and Wu T T 2023 *Chin. Phys. B* **32** 066803
[2] Hwang J J 2013 *Renewable Sustainable Energy Rev.* **19** 220
[3] Pei P, Wang M, Chen D, Ren P and Zhang L 2020 *Prog. Nat. Sci.: Mater. Int.* **30** 751
[4] Hori T, Ma Q, Kobayashi K, Nagao M, Teranishi S and Hibino T 2019 *Int. J. Hydrogen Energy* **44** 2454
[5] Majeed H and Svendsen H F 2018 *Chem. Eng. J. (Amsterdam, Neth.)* **333** 636
[6] Majeed H and Svendsen H F 2018 *Int. J. Greenhouse Gas Control* **74** 282
[7] Meng F, Meng Y, Ju T, Han S, Lin L and Jiang J 2022 *Renewable Sustainable Energy Rev.* **168** 112902
[8] Dutta A, Pan Y, Liu J Q and Kumar A 2021 *Coord. Chem. Rev.* **445** 214074
[9] Liu Q, Yu J and Hu J 2024 *Chin. Phys. B* **33** 017204
[10] Li Y Z, Wang G D, Ma L N, Hou L, Wang Y Y and Zhu Z H 2021 *ACS Appl. Mater. Interfaces* **13** 4102
[11] Gu Y M, Yuan Y Y, Qadir S, Yuan Z S, Zhao S S, Sun T J, Liu X W and Wang S D 2022 *Chem. Eng. J.* **433** 134447
[12] Singh A and Kayal S 2022 *Prot. Met. Phys. Chem. Surf.* **58** 478
[13] Soares E d A, Barreto Jr A G and Tavares F W 2023 *Fluid Phase Equilib.* **574** 113887
[14] Anastasiou I, Van Velthoven N, Tomarelli E, Lombi A, Lanari D, Liu P, Bals S, De Vos D E and Vaccaro L 2020 *ChemSusChem* **13** 2786
[15] Dou Y, Yang L, Qin L, Dong Y, Zhou Z and Zhang D 2021 *J. Solid State Chem.* **293** 121820
[16] Wu L, Zhang X F, Li Z Q and Wu F 2016 *Inorg. Chem. Commun.* **74** 22
[17] Liu W, Xie J, Zhang L, Silver M A and Wang S 2018 *Dalton Trans.* **47** 649
[18] Hosseinzadeh B and Rodriguez-Mendez M L 2023 *Chemosensors* **11** 357
[19] Feng A, Wang Y, Ding J, Xu R and Li X 2021 *Curr. Drug Deliv.* **18** 297
[20] Li C, Chen C, Wei Y, Tan M, Zhai S, Zhao J, Wang L and Dai T 2021 *Drug Delivery* **28** 2594
[21] Zong Z, Tian G, Wang J, Fan C, Yang F and Guo F 2022 *Pharmaceutics* **14** 2790
[22] Mehtab T, Yasin G, Arif M, Shakeel M, Korai R M, Nadeem M, Muhammad N and Lu X 2019 *J. Energy Storage* **21** 632
[23] Zhao W, Zeng Y, Zhao Y and Wu X 2023 *J. Energy Storage* **62** 106934
[24] Zhao G, Xie J, Zhou K, Xing B, Wang X, Tian F, He X and Zhang L 2022 *Chin. Phys. B* **31** 037104
[25] Qiao Z, Zhang K and Jiang J 2016 *J. Mater. Chem. A* **4** 2105
[26] Avci G, Velioglu S and Keskin S 2018 *ACS Appl. Mater. Interfaces* **10** 33693
[27] Li M, Cai W, Wang C and Wu X 2022 *Phys. Chem. Chem. Phys.* **24** 18764
[28] Ryu D and Kim J 2023 *J. Phys. Chem. C* **127** 10384
[29] Willems T F, Rycroft C H, Kazi M, Meza J C and Haranczyk M 2012 *Microporous Mesoporous Mater.* **149** 134
[30] Mayo S L, Olafson B D and Goddard W A 1990 *J. Phys. Chem.* **94** 8897
[31] Rappe A K, Casewit C J, Colwell K S, Goddard W A, III and Skiff W M 1992 *J. Am. Chem. Soc.* **114** 10024
[32] Zhou F, Chen Y, Zhang Z, Gu Z, Sun Y, Tong M, Yang Q, Dong W, Pan Y, Qiao Z and Zhong C 2024 *AIChE J.* **70** e18455
[33] Xu H, Mguni L L, Shan Y, Jewell L L, Hildebrandt D, Yao Y and Liu X 2025 *Sep. Purif. Technol.* **354** 128927
[34] Dokur D and Keskin S 2018 *Ind. Eng. Chem. Res.* **57** 2298
[35] Morales A D C, Economou I G, Peters C J and Siepmann J I 2013 *Mol. Simul.* **39** 1135
[36] Jones J E 1924 *Proc. R. Soc. London A* **106** 441
[37] Yuan J P, Liu X Y, Li X D and Yu J X 2020 *Mater. Today Commun.* **26** 101987
[38] Liu X Y, He J, Yu J X, Li Z X and Fan Z Q 2014 *Chin. Phys. B* **23** 067303
[39] Vlugt T, García-Pérez E, Dubbeldam D, Ban S and Calero S 2008 *J. Chem. Theory Comput.* **4** 1107
[40] Jiang Y C, Li G X, Yu G F, Juan W, Huang S L and Xu G L 2021 *Chin. Phys. B* **30** 118105
[41] Liu X, Liu J, Mao S, Xu H, Wang Y, Tao W and Li Z 2024 *Fluid Phase Equilib.* **581** 114073
[42] Dubbeldam D, Torres-Knoop A and Walton K S 2013 *Mol. Simul.* **39** 1253
[43] Dubbeldam D, Calero S, Ellis D E and Snurr R Q 2016 *Mol. Simul.* **42** 81
[44] Yuan J P, Liu X Y, Li X D and Yu J X 2021 *Acta Phys. Sin.* **70** 156801 (in Chinese)
[45] Yuan J P, Liu X Y, Wang H and Li X D 2023 *Comput. Mater. Sci.* **216** 111872
[46] Liu X Y, Chen H, Yuan J P, Huang J l, Dong L X and Xin Y J 2023 *Z. Naturforsch. A: Phys. Sci.* **78** 863
[47] Mert H, Deniz C U and Baykasoglu C 2023 *J. Mol. Model.* **29** 315
[48] Altundal O F, Altintas C and Keskin S 2020 *J. Mater. Chem. A* **8** 14609
[49] Cen X, Sun Y, Yu C, Geng C, Gu Z, Ao D, Zhang Z, Qiao Z and Zhong C 2024 *Sep. Purif. Technol.* **334** 125995